Microcylinder pump employing $0.57Pb(Sc_{1/2}Nb_{1/2})O_3–0.43PbTiO_3$ piezoelectric actuator

B. PEČAR[a*], H. URŠIČ[b], B. MALIČ[b], M. MOŽEK[a], D. VRTAČNIK[a]
[a]*University of Ljubljana, Faculty of Electrical Engineering, Laboratory of Microsensor Structures and Electronics, Tržaška 25, SI-1000 Ljubljana, Slovenia*
[b]*Electronic Ceramics Department, Jožef Stefan Institute, Jamova 39, SI-1000 Ljubljana, Slovenia*

The microcylinder pumps employing piezoelectric actuators based on relaxor-ferroelectric $0.57Pb(Sc_{1/2}Nb_{1/2})O_3–0.43PbTiO_3$ are fabricated and characterized. The prototypes with 6 mm chamber diameter and with a modified outlet rectifying element feature high water / air flowrate performance (up to 1 ml min^{-1} / up to 3.8 ml min^{-1}) and backpressure performance (up to 215 mbar / up to 65 mbar) at the excitation amplitude of 130 V. To our knowledge, it is the first time the relaxor-ferroelectric material has been employed in a piezoelectric micropump application.

(Received June 17, 2016; accepted October 10, 2017)

Keywords: Micropump, Microcylinder pump, Relaxor based material, PSN-PT, Excitation amplitude

1. Introduction

Piezoelectric actuation was the first actuation principle used for micropumps [1]. It provides a high stroke volume, a high actuation force, fast mechanical response and great repeatability [2]. However, high excitation amplitudes in the order of several hundreds of volts needed for piezoelectric actuation represent a major disadvantage and limit the usability of piezoelectric micropumps in specific portable medical applications, such as in implantable drug-delivery systems [3].

Currently, only few miniaturized piezoelectric micropump driver circuits are available on the market, including mp6-OEM [4] (Bartels Mikrotechnik GmbH, Germany, U_{max}=235 volts peak-to-peak (V_{pp})), MPD-200 [5] (BMT Fluid Control Solutions GmbH, Germany, U_{max}=250 V_{pp}), mpD001 [6] (Fraunhofer EMFT, Germany, U_{max}=320 V_{pp}) and Pump Control Board [7] (Dolomite microfluidics, United Kingdom, U_{max}=160 V_{pp}). Such excitation amplitudes have been found insufficient for efficient performance of polymeric piezoelectric micropumps [8, 9]. To achieve a higher performance at lower excitation amplitudes, numerous micropump design optimizations have been reported in the last decade employing analytical modeling [10], finite-element-method numerical simulations [11] and multi-chamber designs [12].

An effective method for reducing the excitation signal amplitudes in piezoelectric micropumps might be the use of highly efficient piezoelectric materials. In recent years, relaxor-ferroelectrics such as $Pb(Mg_{1/3}Nb_{2/3})O_3–PbTiO_3$, $Pb(Zn_{1/3}Nb_{2/3})O_3–PbTiO_3$ or $Pb(Sc_{1/2}Nb_{1/2})O_3–PbTiO_3$ with morphotropic phase boundary compositions have generated a lot of interest due to its high dielectric permittivity, excellent piezoelectric properties and high electrostriction, which makes them appealing for applications of multilayer capacitors, actuators, sensors, and electro-optical devices [13].

Yamashita [14] and Adachi et al. [15] have shown that niobium-doped $0.57Pb(Sc_{1/2}Nb_{1/2})O_3–0.43PbTiO_3$ (PSN–43PT) exhibits electromechanical coupling and piezoelectric constants that rival those of the most widely used piezoelectric ceramic $Pb(Zr,Ti)O_3$ (PZT) and may prove to be of a high technological interest. Moreover, in our previous work [16,17] we have shown that the functional properties of PSN–43PT ceramics prepared from the mechanochemically derived powder are even better than the properties of niobium-doped PSN–43PT ceramics prepared by conventional solid state synthesis.

In this work, microcylinder pumps employing custom designed high piezoelectricity PSN–43PT actuators were fabricated and characterized. Microcylinder pumps comprise two active rectifying elements, which exploits the specific deformation of glass membrane that is loosely attached via a resilient elastomer to the top of the supporting glass. Rectifying elements efficiency increases with the degree of membrane deformation, therefore flowrate and backpressure performance characteristics increase non-lineary with applied excitation amplitude. This is contrary to conventional passive check valves micropumps where this dependency is linear. Therefore, microcylinder pump requires strong deformation of the membrane at moderate excitation amplitude. This can be assured with relaxor-ferroelectric PSN-43P material that exhibits excellent piezoelectric properties. To the best of our knowledge, it is the first time the relaxor-ferroelectric material has been employed in piezoelectric micropump application.

2. Design of a microcylinder pump

Fig. 1 and Fig. 2 shows a 3-D exploded view and cross-section view of a typical microcylinder pump structure, respectively.

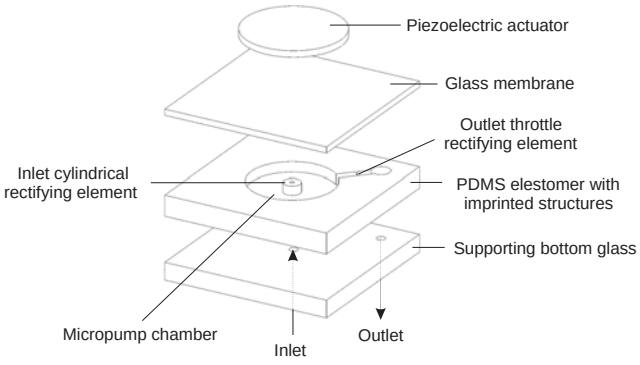

Fig. 1. 3-D exploded view of a typical microcylinder pump structure (dimensions are not to scale)

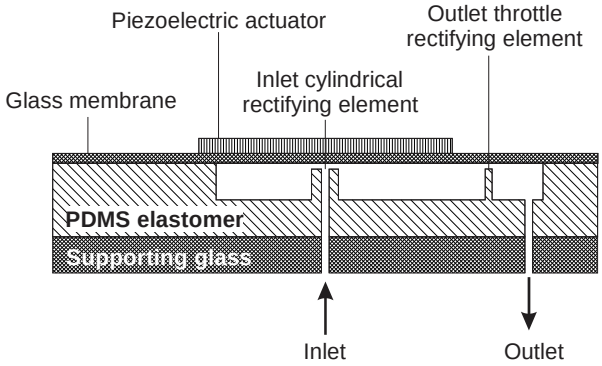

Fig. 2. Microcylinder pump cross-section view (dimensions are not to scale)

Microcylinder pump comprises elastomeric material bonded on its bottom side to the supporting bottom glass. One inlet and one outlet fluid ports are drilled through a thick supporting bottom glass that supply and drain the fluid into and out of the pump. Micropump chamber, fluidic microchannel, inlet cylindrical rectifying element and outlet rectifying element are molded on the upper side of the elastomer. Additionally, two through-holes are punched into an elastomer, one into the center of the micropump chamber and the other one at the end of the channel. The micropump chamber and the microchannel are sealed with a thin glass membrane. Piezoelectric actuator is positioned in the axis of a micropump chamber, coupled rigidly to the micropump membrane.

During excitation the loosely attached glass membrane and elastomer (PDMS) deform in a distinguished manner that enables compression and expansion of the inlet and outlet rectifying element with a phase lag sufficient for proper micropump operation.

Previously reported design [9] comprised step shaped outlet rectifying element with integrated outlet port. Hydraulic resistance of the outlet-rectifying element was defined by the distance between outlet rectifying element step edge and edge of the outlet fluidic port aperture, by gap between edge of the step and membrane and by local deformation of the membrane.

Since the outlet fluidic port aperture is punched manually during fabrication process, the small variation in the position of the aperture can reflects in the inconsistent micropumps flowrate and backpressure performance.

In this work, outlet rectifying element was modified into the shape of throttle and outlet port aperture was moved toward the edge of the micropump, away from the first extreme of membrane deformation.

With such a design, the hydraulic resistance of the outlet rectifying element is defined by the width of the throttle, by throttle gap and by local deformation of the membrane, but not by the position of the outlet port. This approach improves fabrication reproducibility and facilitate fabrication process.

3. Materials and methods

For the synthesis of the PSN–43PT powder, PbO (99.9 %, Aldrich), Sc_2O_3 (99.9 % Alfa 11216), TiO_2 (99.8 %, Alfa Aesar) and Nb_2O_5 (99.9 %, Aldrich) were used. The homogenized, stoichiometric mixture was mechanochemically activated in a high-energy planetary mill (Retsch, ModelPM400) for 24 h at 300 rpm. The powder was heated at 900 °C for 1 h. The powder compacts were pressed isostatically at 300 MPa and sintered in the presence of PSN–43PT packing powder at 1000 °C for 8 h. The density of the sintered ceramics measured with the gas displacement density analyser (Micromeritics, AccuPyc III 1340 Pycnometer) was 7.60 g/cm^3, which is 96 % of the theoretical density 7.94 g/cm^3. After sintering the pellets were cut, polished and annealed at 600 °C. The disks had a diameter of 8 mm and were approximately 200 μm thick.

Cr/Au electrodes were deposited on the faces of the disks by RF-magnetron sputtering (5 Pascal). The poling conditions of PSN–43PT actuators were chosen based on our previous study [17], i.e., DC electric field of 3 kV/mm at 160 °C for 5 min and then field-cooled. After poling the samples were aged for 24 h.

For microstructural investigation, the ceramic samples were mounted in epoxy, ground and polished using standard metallographic techniques and thermally etched at 900 °C for 20 min. The microstructure of the ceramics was examined using scanning electron microscope (SEM, JEOL JSM 5800) and it is shown in inset of Figure 3.

Microcylinder pump comprises sandwich of three layers (glass-PDMS-glass). In this work, the supporting bottom glass, elastomer layer and glass membrane are square in shape (23 mm x 23 mm) with the thicknesses of 1 mm, 600 μm and 170 μm, respectively. The pumping chamber diameter was set to 6 mm. The micropump outlet fluidic channel depth and width were set to 60 μm and 1 mm, respectively. The centrally placed inlet cylindrical port is a hollow cylinder with the outer diameter of 2 mm and inner diameter of 300 μm. The outlet compress zone

and step position [9] were set to 400 μm and 1.7 mm, respectively. The gap between each port and micropump membrane was set to 12 μm.

PDMS cast was fabricated by a soft lithography employing replica molding technique. A PDMS Sylagard® 184 (Dow Corning Corporation) two-part kit consisting of a pre-polymer (base) and a cross-linker (curing agent) mixed at a ratio 20:1 was applied. Silicon mold for PDMS cast was fabricated by a one-step photolithography and Deep Reactive Ion Etching (DRIE). Oxygen plasma activation was used to irreversibly seal (bond) the PDMS layer with the thicker supporting bottom glass and a thin rectangular shaped glass membrane. Fluidic connections were made from thicker PDMS discs and bonded on the same way onto the supporting bottom glass. Micropump is driven by a disk-shaped PZT actuator that was glued on the top of the glass membrane (conductive silver paste EPO-TEK EE129-4, from Epoxy Technology Inc.).

Figure 3 shows the fabricated microcylinder pump prototype with the integrated PSN–43PT actuator.

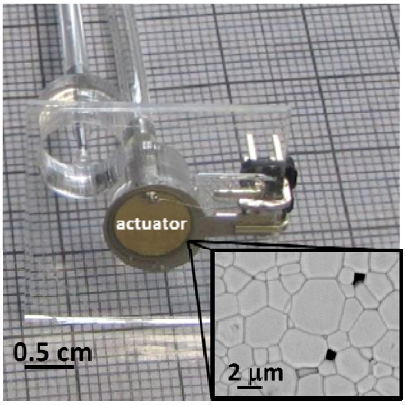

Fig. 3. Piezoelectric micropump with the integrated PSN–43PT actuator. Inset: SEM micrograph of a thermally etched PSN–43PT ceramic.

Material parameters of PSN–43PT are provided in Table 1.

Table 1. Material parameters for piezoelectric actuators

	Mechanochemically derived PSN–43PT [16]
d_{31} (10^{-12} m/V)	260
d_{33} (10^{-12} m/V)	570
$\varepsilon_{33}^{T}/\varepsilon_0$	2200
k_p (%)	71
k_t (%)	56
Q_m	38

A custom built high voltage square waveform generator connected to a PC and a dedicated computer software were employed to automatically drive the micropumps and simultaneously save measured instantaneous flowrate data or back pressure data into computer file. Excitation signal frequency at constant amplitude or vice versa were swept automatically (0-300 Hz with at step of 5 Hz every 10 s and 0-130V with at step of 5 V every 10 s, respectively). Instantaneous water flowrate was computed using gravimetric method ($Q = dm / dt \cdot \rho$) employing a precision scale Kern ABJ 120-4M connected to a PC.

Prior measuring, the water level of collecting tank on the scale was matched with water level of storage tank by placing the latter on laboratory elevator. To minimize evaporation of water from a surface of an open collecting tank, the tank was shaped as a cylinder with a small diameter (1 cm). Falling droplets were avoided by prefilling the collection tank with tare amount of water.

Instantaneous air flowrate was measured with commercial flow sensor Microbridge Mass Airflow Sensor (Honeywell AWM3150V) while instantaneous backpressure / suction pressure of both water and air were measured with calibrated differential pressure sensor (First Sensor AG, HCX005D6V). Both were connected to PC via digital multimeter Keithley 2700.

4. Analytical modeling approach

For positive displacement micropump which employs conventional passive valves the following relations can be given:

$$\Phi, p \overset{linear}{\propto} \varepsilon_{31} \tag{1}$$

Stroke volume and thus micropump flowrate (Φ) and backpressure performance (p) is proportional to the membrane deformation, whereby membrane deformation is proportional to the lateral deformation of the piezoelectric actuator (ε_{31}):

Coupled constituent equations for piezoelectric actuator in strain-charge form reads:

$$\boldsymbol{\varepsilon} = s_E \boldsymbol{\sigma} - d^T \boldsymbol{E} \tag{2}$$

$$\boldsymbol{D} = d\boldsymbol{\sigma} + \varepsilon_0 \varepsilon_{rT} \boldsymbol{E} \tag{3}$$

where $\boldsymbol{\sigma}$ and $\boldsymbol{\varepsilon}$ are stress and strain tensor, respectively. $\boldsymbol{D}$ is electric displacement vector, s_E is the elasticity tensor and ε_{rT} is the relative permittivity tensor. $\boldsymbol{E}$ is electric field proportional to piezoelectric excitation voltage V ($\boldsymbol{E_{31}} \propto V$).

If there is no change in the pump load ($\Delta\sigma = 0$) and no significant change in mechanical properties of the piezoelectric material ($\Delta s_E = 0$), the following applies:

$$\Phi, p \overset{linear}{\propto} d_{31} E_{31} \tag{4}$$

A variation of piezoelectric parameter d_{31} causes a proportional change in conventional passive valve micropump performance characteristics at given electric field E_{31} or given excitation amplitude V .

However, in the case of microcylinder pump, the efficiency of active rectifying elements dependents strongly on membrane deformation. Here, efficiency can be defined as rectifying element hydraulic resistance variation ΔR_h during micropump operating cycle. For outlet throttle implemented in our case, hydraulic resistance variation reads:

$$\Delta R_h \approx \frac{12\eta L}{w(\Delta\varepsilon_{gap})^3(1-0.63\frac{\Delta\varepsilon_{gap}}{w})} \tag{5}$$

where η is fluidic viscosity, w is throttle width, L is throttle thickness and $\Delta\varepsilon_{gap}$ is a gap variation between throttle and the membrane which is proportional to piezoelectric deformation ε_{31}. The efficiency of rectifying elements vs piezoelectric deformation ε_{31} is highly nonlinear. The latter introduces nonlinearity in microcylinder pump flowrate and backpressure response to lateral piezoelectric deformation ε_{31}:

$$\Phi, p \overset{cubic}{\propto} \varepsilon_{31} \tag{6}$$

The equation can be rewritten as:

$$\Phi, p \overset{cubic}{\propto} d_{31}V \tag{7}$$

A small variation of piezoelectric parameter d_{31} at given excitation amplitude causes significant change of maximal microcylinder pump flowrate Φ and backpressure p performance.

5. Results

Fig. 4 shows the typical measured performance characteristics for PSN–43PT microcylinder pumps as a function of excitation frequency and amplitude. In all cases, a square excitation waveform was applied. For the flowrate and backpressure performance vs. excitation signal amplitude measurements (see Fig. 4, b & d), the frequency was tuned for the peak performance with respect to the medium.

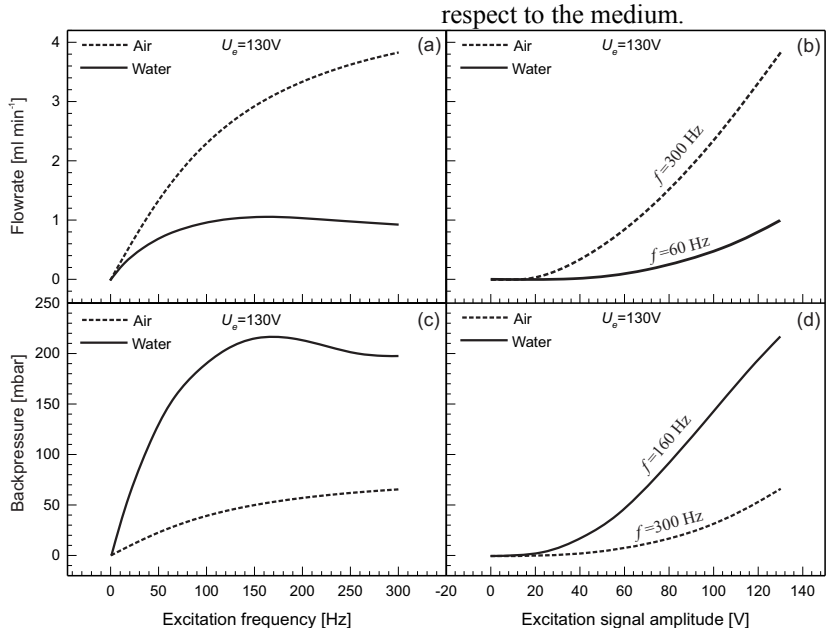

Fig. 4. Typical measured flowrate vs. excitation (a) frequency, (b) amplitude and backpressure vs. excitation (c) frequency and (d) amplitude for PSN–43PT prototypes (media: DI water / air).

Maximum flowrate and the resonance frequency strongly depend on the media viscosity. The water flowrate characteristics (see Fig. 4, a) increase exponentially up to 170 Hz reaching their maximum values of 1 ml min^{-1}. By increasing the excitation frequency, the water flowrate characteristics gradually decline.

In our previous work [9], the water flowrate characteristics for the microcylinder pumps employing the chambers with a diameter of 8 mm (in this work 6 mm) and PZT actuators with a diameter of 10 mm (in this work 8 mm), reach the maximum values at 90 Hz. The higher micropump resonance frequency for water observed in this work is attributed to the smaller pumping chambers and piezoelectric actuators.

The measured air flowrate characteristics (Figure 4, a) do not exhibit any distinct peaks over the frequency measurement interval as they are located above the excitation frequency limit of the measurement setup. Air flowrate characteristics reach maximum of 3.8 ml min^{-1}.

Micropump flowrate performance is closely related to the level of membrane deformation. In elastomeric

microcylinder pumps, the level of membrane deformation dictates both the stroke volume and the efficiency of rectifying elements. Only after the membrane deformation level becomes sufficient, the nonzero flowrate and backpressure at micropump outlet are established.

Micropumps flowrate and backpressure performance are insignificant up to a threshold excitation amplitude. The flowrate threshold excitation amplitude for water is located at 40 V (see Figure 4, b). The air flowrates are rather insignificant up to the threshold excitation amplitude of 10 V. After the membrane deformation becomes sufficient, the flowrate performance increases exponentially with the increased excitation signal amplitude. The water and air flowrate performance characteristics reach 0.95 ml min^{-1} and 3.8 ml min^{-1} at maximum applied excitation amplitudes, respectively.

In our previous work [9, 18], flowrate characteristics of monoactuator peristaltic (MAP) micropumps and microcylinder pumps (MCPs) employing conventional PZT actuator leveled off at amplitudes greater than 230 V (independently on the pumping medium). At such applied excitation amplitudes the polarization saturation occurs which results also in maximal possible membrane displacement and flowrate saturation [19].

In this work, no flowrate saturation trend is observed, which implies that by applying excitation amplitudes up to 130 V for PSN–43PT actuator, the polarization saturation of piezoelectric ceramics did not occur. However, electric field at 130V excitation amplitude for 200 μm thick PSN-PT ceramic disc is about 6.5 kV cm^{-1} what is above or very close to the coercive field of PSN-PT published previously for such material. It is 5-7 kV cm^{-1} in [14, 15] or 10 kV cm^{-1} in [16, 17]. Such high ac electric field might generate depoling of PSN-PT (piezoelectric ceramics is very sensitive to high ac fields) and gradual loss of piezoelectric properties. However, during several measurement repetitions, no measurable performance degradation was observed.

Typical water and air backpressure characteristics as a function of an excitation frequency in the range from 0 Hz to 300 Hz are shown in figure 4, c.

Due to air compressibility and lower rectifying elements efficiency for air, air backpressure performance is lower compared to water backpressure performance. Water backpressure characteristics increase exponentially up to 170 Hz reaching their maximum values of 215 mbar and gradually decline with increased frequency.

Measured air backpressure characteristics do again not exhibit any distinct peaks as found for water due to excitation frequency limit of measurement setup. Air backpressure characteristics reach maximum of 65 mbar.

Fig. 4, d presents typical measured water and air backpressure characteristics as a function of an excitation amplitude. Excitation frequency was tuned for peak performance with respect to the fluid media (see Fig. 4, c).

Backpressure performance characteristics increase exponentially with increased excitation signal amplitude. Water and air flowrate performance characteristic reaches the value of 220 mbar and 65 mbar at maximum applied excitation amplitude of 130 V, respectively.

5.1. Performance comparison to similar reported PDMS micropumps

Table 2 presents a comparison with other similar PDMS micropumps. Superior backpressure and flowrate performance at 130V excitation signal amplitude has was obtained by presented micropumps despite the smallest piezoelectric disk diameter.

Table 2. Performance characteristics of single actuator peristaltic micropumps for water medium

Author, year	Excitation signal amplitude [V]	Rectifying elements	Φ_{water} [ml min^{-1}]	Δp_{water} [mbar]	Piezoelectric actuator	Piezoelectric actuator dimensions
I. D. Johnston et al. (2004)	180	throttles	300	55	PZT disc	na
I. D. Johnston et al. (2005)	130	throttles	350	170	two layer PZT bending disc	diameter: 12.7 mm thickness: 205 μm + 205 μm
M C Tracey et al. (2006)	130	throttles	780 (parallel)	200 (serial)	two layer PZT bending disc	diameter: 12.7 mm thickness: 205 μm + 205 μm
B. Pečar at al. (2013)	130	throttles	80	120	PZT plate	dimension: 25mm x 6.5mm thickness: 200 μm
T. Dolžan et al. (2015)	130	cylinder throttle	800	200	PZT disc	diameter: 10 mm thickness: 200 μm
This work	**130**	cylinder throttle	**1000**	**220**	**PSN-43PT disc**	**diameter: 8 mm thickness: 200 μm**

6. Conclusions

The dependence of piezoelectric micropumps on high excitation amplitudes will become a bottleneck of portable applications. In order to obtain a desirable flowrate and backpressure performance of piezoelectric micropumps at lower excitation amplitudes, the microcylinder pumps employing custom designed PSN–43PT piezoelectric actuators were fabricated and characterized. The fabricated prototypes with 6 mm chamber diameter and with modified outlet rectifying element featured high water / air flowrate performance (up to 1 ml min^{-1} / up to 3.8 ml min^{-1}) and backpressure performance (up to 215 mbar / up to 65 mbar) at excitation amplitude of 130 V.

The performance results indicate that PSN–43PT is a promising material for high performance portable, wearable or implantable micropump applications, where operation amplitude has to be kept low for reasons of safety and smaller plus more economic driver circuits.

This work can stimulate further research on relaxor-ferroelectric materials for use in micropumps of the new generation. The chemical composition, microstructure and domain configuration of relaxor-ferroelectric materials can be further optimized aiming to obtain even better performance of micropump systems including operation at elevated temperatures.

Acknowledgements

Authors would like to thank the Slovenian Research Agency/ARRS (P2-0105, P2-0244) and Ministry of Education, Science and Sport for their support of this work.

References

[1] J. L. J. Thomas, S. P. Bessman, ASAIO Journal, **21**(1), 516 (1975).
[2] J. Kan, K. Tang, G. Liu, G. Zhu, C. Shao, Sensor. Actuat. A-Phys. **144**(2), 321 (2008).
[3] P. Woias, Sensor. Actuat. B-Chem. **105**(1), 28 (2005).
[4] http://www.bartels-mikrotechnik.de/
[5] http://www.pumpen-ventile.de/
[6] http://www.emft.fraunhofer.de/
[7] http://www.dolomite-microfluidics.com/
[8] T. Fujiwara, I. D. Johnston, M. C. Tracey, C. K. L. Tan, J. Micromech. Microeng. **20**(6), 1 (2010).
[9] T. Dolžan, B. Pečar, M. Možek, D. Resnik, D. Vrtačnik, Sensor. Actuat. A-Phys. **233,** 548 (2015).
[10] C. J. Morris, F. K. Forster, J. Micromech. Microeng. **10**(3), 459 (2000).
[11] Q. Cui, C. Liu, X. F. Zha, Int. J. Adv. Manuf. Tech. **36,** 516 (2008).
[12] J. Kan, K. Tang, G. Liu, G. Zhu, C. Shao, Sensor. Actuat. A-Phys. **144**(2), 321 (2008).
[13] S. E. Park, T. R. Shrout, J. Appl. Phys. **82**, 1804 (1997).
[14] Y. Yamashita, Jpn. J. Appl. Phys. **32,** 5036 (1993).
[15] M. Adachi, T. Toshima, M. Takahashi, Y. Yamashita, A. Kawabata, Jpn. J. Appl. Phys. **34,** 5324 (1995).
[16] H. Uršič, J. Tellier, J. Holc, S. Drnovšek, M. Kosec, J. Eur. Ceram. Soc. **32**(2), 449 (2012).
[17] H. Uršič, J. Holc, M. Kosec, J. Eur. Ceram. Soc. **33**(4), 795 (2013).
[18] B. Pečar, D. Križaj, D. Vrtačnik, D. Resnik, T. Dolžan, M. Možek, J. Micromech. Microeng. **24**(10), 105010 (2014).
[19] K. C. Kao, Dielectric phenomena in solids, Elsevier Academic, San Diego (2004).

*Corresponding author: borut.pecar@fe.uni-lj.si